PCCP

ROYAL SOCIETY OF CHEMISTRY

PAPER

View Article Online
View Journal | View Issue

Cite this: *Phys. Chem. Chem. Phys.*, 2023, **25**, 1677

Metal cluster plasmons analyzed by energy-resolved photoemission†

N. Iwe, [a] K. Raspe, [a] F. Martinez,[a] L. Schweikhard,[b] K.-H. Meiwes-Broer[ac] and J. Tiggesbäumker *[ac]

Received 19th August 2022,
Accepted 6th December 2022

DOI: 10.1039/d2cp03830g

rsc.li/pccp

The optical response of size-selected metal clusters is studied by wavelength-dependent photoemission and energy-resolved photoelectron detection. Relative photodetachment cross sections giving information on the plasmon are determined for the example of closed-shell Ag_{91}^-. Notably, the peak energy of this anion (3.74 eV) is higher than the small particle limit in Mie theory of 3.5 eV. Different methods to extract cross sections from the spectra are applied. In particular, we compare the results obtained by integrating the full electron yields to analyses based on evaluating specified binding energy windows. The approach opens up new possibilities to conduct studies on Landau fragmentation as a result of multielectron excitations.

1 Introduction

Novel properties of matter arising from unique structures at the nanoscale are of high interest for scientific research and applications.[1] Composites which comprise nanoparticles offer interesting opportunities to build up functional materials, which, *e.g.*, provide an effective coupling between nanooptics and catalysis.[2] In particular, the optical response of metal nanoparticles, *i.e.* the Mie plasmon resonance,[3] and their use in nanoplasmonics is appealing, because it may be used for improved light guiding and trapping, *e.g.* in thin-film solar cells[4] and for nanoscale focusing in tapered waveguides,[5] or nanoscale antennas.[6] In order to exploit the possibilities in the context of complex materials, it is essential to explore the optical properties of the elementary building blocks, which includes the plasmonics of free metal clusters. By controlling particle size and charge state, unique optical fingerprints can be realized, that provide avenues to design dedicated materials.

The electronic properties of metal particles[7] and fullerenes[8,9] can be well-described by the response of nearly-free electrons within the context of the jellium model. Alkali clusters, *e.g.*, show a collective resonance of the valence electrons down to cluster sizes of $N = 8$.[10,11] It is well-known that the plasmon energies $\hbar\omega_{\mathrm{alkali}}$ show a red-shift as a function of decreasing radius R.[12–14] This phenomenon is related to the electron spill-out δ.[15] In a first order treatment, the resulting increase in the static polarizability α from the classical metallic sphere result R^3 to $(R+\delta)^3$ leads to a ratio between the plasmon frequency of the alkali clusters $\omega_{\mathrm{alkali}}(R)$ and the small particle limit $\hbar\omega_{\mathrm{Mie}}$ of[16]

$$\frac{\omega_{\mathrm{alkali}}(R)}{\omega_{\mathrm{Mie}}} = \sqrt{\frac{\alpha_{\mathrm{Mie}}}{\alpha_{\mathrm{alkali}}(R)}} = \sqrt{\frac{R^3}{(R+\delta)^3}}. \quad (1)$$

Within Mie theory[3] the value of ω_{Mie} can be calculated from the optical constants.[17] Eqn (1) well-describes the size-dependence of the plasmon energy in alkali clusters. The optical response has been studied as function of ellipsoidal deformation,[18,19] temperature[20] and oxidation.[21] Calculations on different theoretical levels are capable to reproduce the experimental findings.[22–25]

Coinage metals and in particular silver particles are also known to exhibit distinct plasmon resonances. Due to the influence of the d-electrons, however, the optical constants modify[17] and the peak in silver shifts from the free-electron value ω_{Mie} to $\hbar\omega_{\mathrm{Mie}}^{\mathrm{Ag}} = 3.5$ eV.[26] In contrast to alkali clusters, Ag_N^+ shows a blue-shift of the resonance with decreasing N, that can be understood, when taking into account the reduced *sd*-screening near the particle surface.[27–29] One finds[27]:

$$\frac{\omega_{\mathrm{silver}}(R)}{\omega_{\mathrm{Mie}}^{\mathrm{Ag}}} = 1 - \frac{1}{2}\left(\frac{\omega_{\mathrm{S}}}{\omega_{\mathrm{Mie}}^{\mathrm{Ag}}}\right)^2 \frac{D_{\mathrm{M}}}{R} \quad (2)$$

where $\hbar\omega_{\mathrm{S}} = 3.7$ eV is the corrected surface plasmon energy and $D_{\mathrm{M}} = -0.8$ Å the *sd*-screening parameter. Whereas eqn (2) describes the development of the plasmon energies in Ag_N^+, the situation for anions is different as they show a red-shift with decreasing size.[30] This particular behavior motivates a more thorough study of the plasmon energy development in silver cluster anions.

[a] *Institute of Physics, University of Rostock, 18059, Rostock, Germany. E-mail: josef.tiggesbaeumker@uni-rostock.de*
[b] *Institute of Physics, University of Greifswald, 17489, Greifswald, Germany*
[c] *Department Life, Light and Matter, University of Rostock, 18059, Rostock, Germany*

† Electronic supplementary information (ESI) available. See DOI: https://doi.org/10.1039/d2cp03830g

Even up to date, the method of choice to measure optical spectra of anionic clusters is to record photodepletion yields.[31] The corresponding signals are extracted by measuring photoreaction yields, that is

$$\begin{aligned} \mathrm{Ag}_N^- + \hbar\omega &\rightarrow \mathrm{Ag}_N + \mathrm{e}^- \\ &\rightarrow \mathrm{Ag}_{N-m}^- + \mathrm{Ag}_m \end{aligned} \quad (3)$$

A drawback of the photodepletion method is that essential details of the cluster response are lost, *i.e.*, the coupling to the electronic system triggered by the photoabsorption is not accessible. In contrast, recording the corresponding photoelectron spectra will provide this information.

In this contribution, we record photoelectron spectra of silver cluster anions of size $N = 91$ in order to obtain relative photodetachment cross sections, *i.e.* differential cross sections with respect to the energy of the emitted photoelectrons. To the best of our knowledge, such a treatment was not utilized before to obtain an extended characterization of the plasmonic response of metal clusters. Further, the method presented here will enable us to capture the optical response of a broader class of systems, namely polyanionic clusters.

2 Experimental setup

Details about the experimental setup have been published elsewhere.[32] Briefly, a magnetron-based gas aggregation source is used to produce a molecular beam of clusters, which contains negatively charged silver cluster anions.[33] After size-selection, the particles enter a digital radio frequency ion trap,[34] where the anions are accumulated using argon buffer gas cooling. By pulsed extraction at a rate of 10 Hz, the anions are transferred into the interaction region, where light from a tunable laser system illuminates the cluster bunch. An optical parametric oscillator (OPO) laser system delivers nanosecond light pulses between $E_{\mathrm{ph}} = 3.52$–4.11 eV at pulse energies on the order of 1 μJ. The OPO process, however, comes along with considerable pulse-to-pulse fluctuations. Therefore, electron signals and pulse energies are monitored on a shot-to-shot basis. This allows for a compensation of pulse fluctuations in the data evaluation, thus ensuring the determination of reliable response cross sections. Photon fluxes are adjusted with respect to changes in the photodetachment cross sections. The entire energy-resolved photoelectron signals are obtained by a magnetic bottle electron spectrometer.[35] Special care was taken in the calibration procedure to minimize artificial electron binding energy shifts, when changing the laser wavelength.[32]

3 Results

The photoelectron measurements were conducted on Ag_{91}^-. This particular size was chosen for two reasons: (i) according to jellium calculations a metal cluster having $N_e = 92$ valence electrons represents a closed-shell system.[15] Such magic clusters are expected to have a spherical shape and thus should

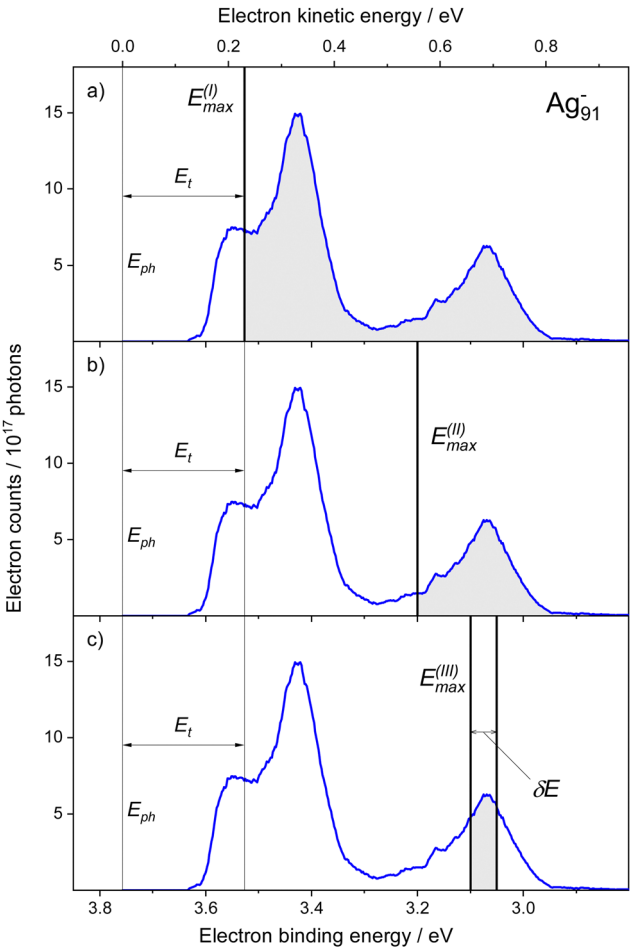

Fig. 1 Experimental photoelectron energy spectrum of Ag_{91}^- (blue line), obtained at $E_{\mathrm{ph}} = 3.76$ eV. The panels (a–c) illustrate three different methods to analyze the spectrum and determine relative photodetachment cross sections, see corresponding shaded regions. (a) The signals are integrated up to a photon-energy dependent binding energy value of $E_{\mathrm{max}}^{(\mathrm{I})} = E_{\mathrm{ph}} - E_{\mathrm{t}}$. E_{t} marks the energy range, where the transmission of the spectrometer decreases significantly (Method I). Note that the excluded binding energy range may contain substantially more electrons than registered in the above plot (Fig. S1, ESI†) (b) irrespective of the photon energy, the electron yields are summed up to a selected maximum binding energy value $E_{\mathrm{max}}^{(\mathrm{II})}$ (Method II); (c) the spectrum is integrated only within a selected narrow binding energy region, *i.e.* $[E_{\mathrm{max}}^{(\mathrm{III})} - \delta E;\ E_{\mathrm{max}}^{(\mathrm{III})}]$ (Method III).

reveal only a single plasmon peak.[16] (ii) The onset of photoemission, characterized by the electron affinity $E_{\mathrm{A}} = 3.03$ eV,[36] is low compared to larger cluster anions.[36] Thus, an excitation energy range, which extents to lower E_{ph} can be captured to determine detachment cross sections. Fig. 1a shows the electron spectrum taken at $E_{\mathrm{ph}} = 3.76$ eV. The onset of photoemission is found at an electron binding energy E_{bin} of around 2.95 eV, followed by a first peak at 3.07 eV and a second one at $E_{\mathrm{bin}} = 3.42$ eV. The overall structure compares well with previous studies of other groups.[37] At a binding energy of almost 3.6 eV the signal decreases substantially, which originates from the low detection efficiency of the spectrometer for slow electrons, We take this into account by defining a minimum detection threshold for the electron kinetic energy of

E_t = 0.23 eV (Fig. 1). Thus, signals for $E_{bin} > E_{ph} - E_t$ are excluded from further evaluation.

The single-shot data acquisition, where both, the laser pulse energy and the photoelectron yield, are recorded, enables us to analyze the data as shown in Fig. 2: a linear function is fitted to the number of electrons detected and plotted *versus* the number of photons. From the resulting slopes relative photodetachment cross section are determined. Note that conducting the analysis in such a way has the advantage, that offsets in the determination of the pulse energies and/or electron counts (*e.g.* due to dark counts of the detector), see intersections with the ordinate, have no effect on the extracted cross sections.

In the core of the subsequent evaluation, we concentrate on the photon energy dependent cross sections, which are also a function of the binding-energy range. For this reason, we specify three methods and analyze:

- The entire photoelectron spectra up to the highest accessible E_{bin}, *i.e.* $E_{max}^{(I)} = E_{ph} - E_t$ (Fig. 1a).
- The photoelectron spectra up to a predefined maximum binding energy $E_{max}^{(II)}$ (Fig. 1b).
- The photoelectron spectra only within a selected energy window δE, *i.e.* in the range $[E_{max}^{(III)} - \delta E; E_{max}^{(III)}]$ (Fig. 1c).

Note that only $E_{max}^{(I)}$ depends on E_{ph}, whereas $E_{max}^{(II)}$ and $E_{max}^{(III)}$ are constant values to be defined.

3.1 Method I

Evaluation of the entire spectrum (Method I) allows for a comparison to corresponding photodepletion experiments, whereby one has to take into account that photo-induced cluster fragmentation is not captured. The cross sections σ_I from wavelength-dependent measurements are shown in Fig. 3 (open symbols). Inspecting σ_I, a clear increase in the optical response is obtained at energies between E_{ph} = 3.58 eV and 3.78 eV. The cross sections show a broad feature, that decreases slowly for energies above 3.85 eV. Backed by results obtained by photodepletion,[30,38] photoionization[39,40] and photoabsorption[26,41,42] experiments on unsupported Ag clusters and nanoparticles, the feature can be assigned to a collective response of the valence electrons. As indicated in Fig. 1, electrons having kinetic energies below E_t are excluded from the analysis, due to the reduced detection efficiency with respect to low energy electrons. Consequently, the cross-section values may be largely underestimated especially at lower photon energies, leading to an artificial peak shift towards higher energies. In fact, in photodepletion restricted to electron emission (see eqn (3)), the entire electron spectrum has to contribute when determining the optical response. In order to obtain more reliable values, a representative photoelectron spectrum taken at the highest photon energy of E_{ph}^{max} = 4.11 eV is used to "complete" the spectra recorded at photon energies $E_{ph} < E_{ph}^{max} - E_t$ = 3.88 eV. We thereby assume no qualitative change of the spectra with E_{ph}. Thus, one can estimate the fraction of the electron yield Y within the critical energy window $[E_{ph} - E_t; E_{ph}]$ and correct the previously obtained cross sections with a corresponding factor

$$C(E_{ph}) = \frac{\int_0^{E_{ph}} Y(E_{ph}^{max}) dE_{bin}}{\int_0^{E_{ph}-E_t} Y(E_{ph}^{max}) dE_{bin}} \quad (4)$$

Conducting the analysis in such a way leads to the corrected cross sections presented in Fig. 3 (closed symbols). Fitting a Lorentz profile to the data results in a plasmon peak position at 3.76 eV. By consideration of the correction procedure, the cross sections increase by up to a factor of eight, which is due to the large proportion of electrons located at high binding energies above 3.3 eV (Fig. S1, ESI†). One should therefore note that a significant number of low energy electrons showing up in the binding energy region $[E_{ph} - E_t; E_{ph}]$ may lead to a noticeable shift of the cross section values. Possible qualitative changes of the

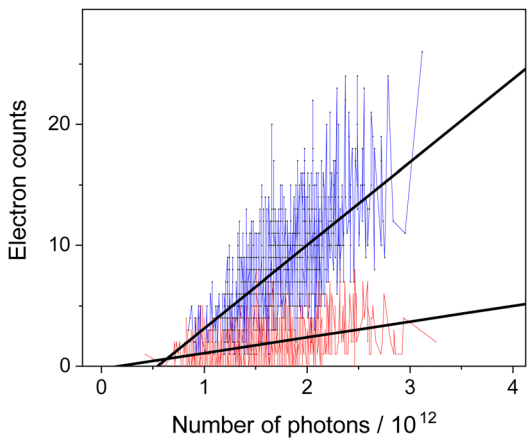

Fig. 2 Number of electrons per laser shot *vs.* number of photons, exemplary shown for two selected photon energies (red: 3.92 eV, blue: 3.76 eV). Slopes obtained from linear fitting (black) provide measures of the relative photodetachment cross sections. The experimental data points are plotted as connected lines for better clarity.

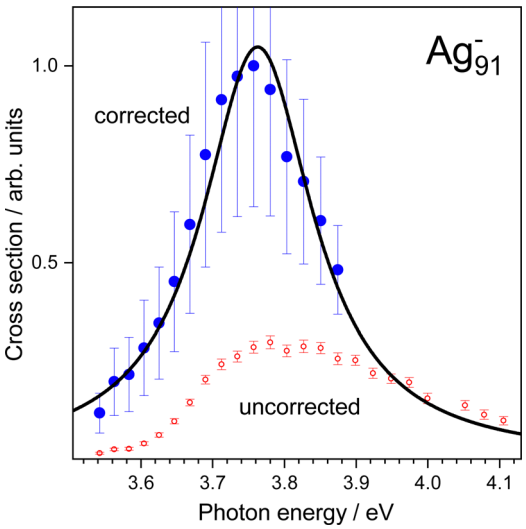

Fig. 3 Photon energy dependent electron detachment cross sections obtained for Ag_{91}^-. The photoelectron signals were evaluated up to $E_{bin} = E_{ph} - E_t$ (Method I, open symbols). Correcting the data for contributions from low-energy electrons ($0 < E_{kin} < E_t$), the actual photodepletion cross sections are estimated (closed symbols). Note the increase in the error margins due to the correction procedure. See text for details.

spectra with photon energy are also not covered. These contributions, however, could have a significant impact on the resulting cross sections and hence represent a drawback of the procedure.

3.2 Method II

While Method I represents a complex data analysis, the results allow for a direct comparison with other depletion experiments. However, the approach comes along with some disadvantages. In order to bypass the correction procedure and thus avoid systematic errors in the detection method, it is advisable to concentrate on a limited energy range in the evaluation (Fig. 1b). In the implementation of Method II, we assume that the selected range of E_{bin} adequately maps the cross sections. Electron signals are evaluated up to a predefined binding energy $E_{max}^{(II)}$. Excitation energies are thereby restricted to $E_{ph} \geq E_{max} + E_t$. This ensures that the specified binding energy window is fully covered for all E_{ph}.

Resulting detachment cross sections σ_{II} for selected $E_{max}^{(II)}$ values are presented in Fig. 4. We notice, that:

- all energy windows show a similar development of σ_{II}.
- choosing the value of $E_{max}^{(II)}$ too small leads to significant uncertainties with respect to σ_{II} due to lower statistics (a).
- the statistical uncertainty reduces when increasing the energy window (a–c). However, cross sections at lower excitation energies are not captured for too large $E_{max}^{(II)}$ (c).

3.3 Method III

Finally, the electron spectra were evaluated by using Method III. The procedure is similar to Method II, but now the energy window is tuned to specific needs, *i.e.* $[E_{max}^{(III)} - \delta E; E_{max}^{(III)}]$, see Fig. 1c. This enables us to resolve photon energy dependencies of the cross sections for different binding energy regions. In order to illustrate Method III, a $\delta E = 50$ meV broad slice of the low binding energy peak is selected, see Fig. 1, and analyzed with respect to electron detachment. The corresponding cross sections are presented in Fig. 4d. Clearly, the development of the data points as obtained by Method I (Fig. 3) and II (Fig. 4a–c) is well-reproduced although the energy window used for the evaluation is significantly restricted.

Fig. 5 summarizes the collective resonance energies determined by applying Methods I–III. Although different evaluation techniques are used, the Methods II and III provide a reliable plasmon energy of 3.73 eV. Note that analyzing different regions of the low binding energy peak using Method III shows almost no shift of the plasmon. Clearly, the plasmon energy of Ag_{91}^- neither depends on the chosen values of E_{max} nor on the method applied. As long as the envelope of the resonance is sufficiently sampled, a conclusive fit curve can be obtained, see also Fig. 4. The plasmon energy value obtained by Method I of 3.76 eV, is only about 30 meV higher, which is probably a result of the increased uncertainty due to the correction as discussed.

4 Discussion

In our photoreaction experiment on Ag_{91}^- only a single reaction pathway, *i.e.* photodetachment of electrons, is considered,

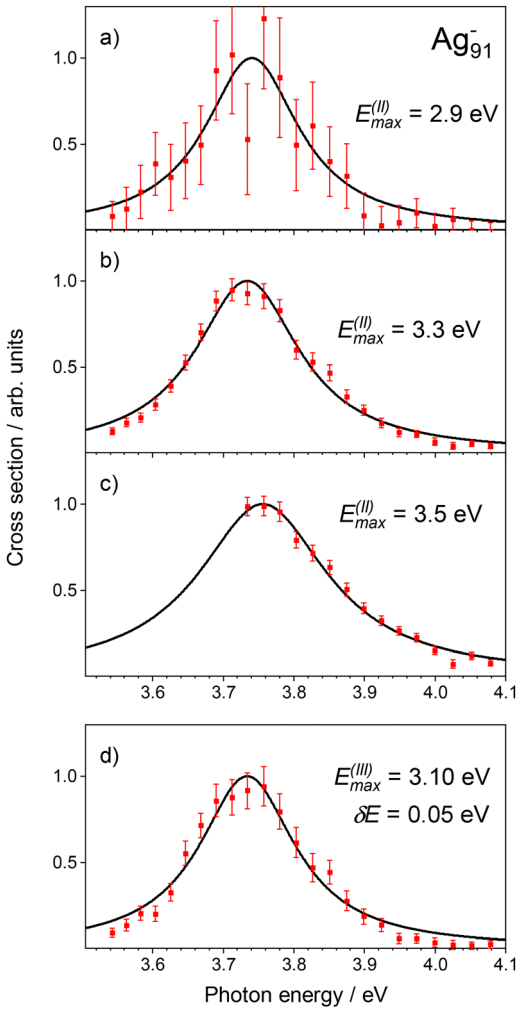

Fig. 4 Photoelectron cross sections of Ag_{91}^- (red dots) with Lorentz fit functions (black lines). The photoelectron signals were evaluated up to a predefined maximum binding energy $E_{max}^{(II)}$ as indicated (Method II, a–c) and in a defined binding energy range between 3.05 and 3.10 eV (Method III, d).

but other processes may contribute as well. This raises the issue of the coupling of the collective electron motion to single particle states termed Landau damping.[43] Indeed, fluorescence as a corresponding plasmon decay channel has been found, however, for only a few clusters like Ag_8.[44] This process requires excited-state lifetimes on the order of nanoseconds. Such exceptional long lifetimes are not expected for metal clusters in general due to the high density of electronic states. This statement is supported by experiments on supported Ag clusters, where lifetimes in the femtosecond regime have been reported.[45] The excess energy may also dissipate into other internal degrees of freedom, potentially leading to the evaporation of atoms. Indeed, in plasmon measurements on Na_{91}^-, photofragmentation has been identified as competing decay channel to photodetachment.[31] Moreover, at higher photon energies, photoemission is almost suppressed. If the excitation leads to a heating of the electron system, single electron emission does not take place. The coupling of the electronic

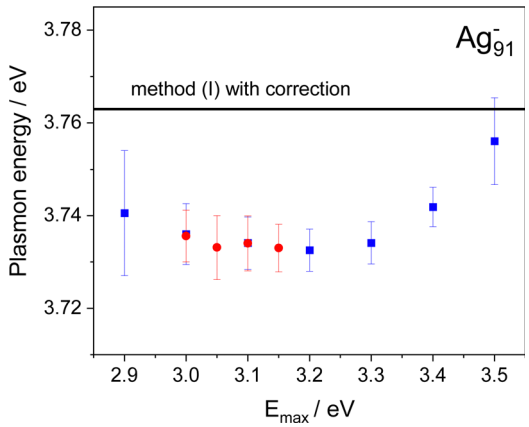

Fig. 5 Comparison of the plasmon energy obtained from the different data evaluation methods described in the text. The photoelectron signal was either analyzed up to $E_{bin} = E^{(II)}_{max}$ (blue square) or in separated binding energy windows $[E^{(III)}_{max} - \delta E; E^{(III)}_{max}]$ (δE = 50 meV) (red circles), see Fig. 4. The low-energy cutoff of the spectrometer limits the electron transmission, which requires a correction procedure for Method I, see Fig. 3 and text for details. The solid line shows the corresponding corrected value, when using the entire electron signal. Note that when determining the error margins, only statistical errors were taken into account.

excitation to vibrational modes finally results in an evaporation of atoms, which has been observed for small silver clusters on time scales extending up to several milliseconds.[46–48] Time-dependent local-density approximation (TDLDA) calculations on Na_N have shown that Landau damping contributes beyond $N = 92$.[22] In our experiments, we cannot exclude photofragmentation.[49] Probably, the increase in the density of single electron states with cluster size[50] favors extensive Landau damping into many electron–hole states. Further energy dissipation into vibratioal modes finally triggers cluster fragmentation. Analyzing photoemission signals in specific energy ranges may provide further insights into relaxation pathways. With the availability of ultrashort laser pulses[51] it has even become possible to trace the electronic response on ultrafast time scales, *i.e.* conducting time-resolved photoelectron spectroscopy.[52,53]

The plasmon energies of free, supported and embedded silver nanoparticles have been studied in detail experimentally[39,54–57] as well as by theory.[58–66] By considering the respective matrix shifts, experiments on size-selected Ag clusters embedded in rare gases confirm the results obtained in the molecular beam.[57] An interesting dependence is obtained, when comparing clusters of different charge state, keeping the relevant number of valence electrons constant. In Ag_8[39,40] and Ag_9^{+}[38] the position hardly shifts, whereas in Ag_7^{-} the plasmon lowers in energy by 0.68 eV with respect to Ag_9^{+} and centers at 3.34 eV.[30] Interestingly, our result for Ag_{91}^{-} (3.73 eV) overshoots the small particle limit $\hbar\omega^{Ag}_{Mie}$ of 3.5 eV and tends to coincide with the result of 3.74 eV expected for Ag_{91}^{+} (eqn (2)). Possibly, the Ag cluster charge state has hardly any influence on the plasmon energies in this size range, which is in contrast to the behavior of sodium clusters of similar size.[14,31] Followup experiments on the cluster anion size dependence are under way, which will clarify, whether the plasmon energies in larger Ag_N^{-} indeed develop similar to those of cationic systems.[27] Evidence for the applicability of eqn (2) to larger systems, independent of their charge state, stems from photoabsorption measurements on unsupported 2 nm silver nanoparticles.[41]

All methods described in the present work can be applied in parallel, since the values are determined after the data sets have been recorded. Method I is closest to photodepletion and thus provides the traditional measure of the absorption cross sections. However, for a full analysis, measurements on the competing decay channel of photofragmentation have to be conducted, too. To get access to the entire photoelectron signal, the detection efficiency of magnetic bottle spectrometers at low electron energies has to be improved. This can be accomplished by accelerating the electrons by a weak electrostatic potential.[32,67] Method II is based on the assumption that photodetachment fully reflects in the evolution of the weakly bound electrons and that therefore the evaluated signals are good measures of the actual cross sections. As an advantage, only the signals close to the detachment energy threshold are evaluated. Compared to Method I, the yields in the selected low binding energy region depend to a lesser extent on spectrometer transmission. As demonstrated by Fig. 4 and 5, the analysis allows to adjust $E^{(II)}_{max}$ in a proper way. In our experiment on Ag_{91}^{-} (E_A = 3.03 eV), which covers a photon energy range between 3.52 and 4.11 eV, E^{II}_{max} = 3.3 eV is an appropriate choice. Method III in principle allows to study the wavelength dependence of selected photoelectron peaks. It is well-known from other experiments, that inelastic energy loss, shake-up, and autodetachment can modify the spectra.[68] Method III reveals the differential cross section with respect to the photoelectron energy and, thus, in principle allows for investigating such processes.

5 Conclusions

In summary, a procedure has been described, which allows to determine relative photodetachment cross sections of silver cluster anions in various ways, providing information on the optical response with respect to direct photoemission. The methods of evaluation are not restricted to metal nanoparticles but can be applied to other systems as well. For example, the present studies could be extended to the optical response of polyanionic molecules, which are relevant to photochemistry.[69] In contrast to photodepletion, photoelectron spectroscopy allows to separate direct electron emission from processes like fragmentation, which develop on longer time scales. Evaluating plasmon-induced photoemission is thereby of utmost importance for applications like photocatalysis[70] and photovoltaics.[71] Understanding the fundamentals of plasmon decay into hot electrons in metal nanoparticles and nanostructures offers promising prospects for efficient energy conversion of light.

Conflicts of interest

There are no conflicts to declare.

Acknowledgements

We would like to thank Madlen Müller for helpful discussions. S. Lochbrunner provided us with a tunable laser system. The Deutsche Forschungsgemeinschaft (TI 210-10) is gratefully acknowledged for financial support.

References

1 E. Roduner, Size matters: Why nanomaterials are different, *Chem. Soc. Rev.*, 2006, **35**, 583–592.
2 M. Valenti, M. P. Jonsson, G. Biskos, A. Schmidt-Ott and W. A. Smith, Plasmonic nanoparticle-semiconductor composites for efficient solar water splitting, *J. Mater. Chem. A*, 2016, **4**, 17891–17912.
3 G. Mie, Beiträge zur Optik trüber Medien, speziell kolloidaler Metalllösungen, *Ann. Phys.*, 1908, **25**, 377–445.
4 C. Clavero, Plasmon-induced hot-electron generation at nanoparticle/metal-oxide interfaces for photovoltaic and photocatalytic devices, *Nat. Photonics*, 2014, **8**, 95–103.
5 M. I. Stockman, Nanofocusing of Optical Energy in Tapered Plasmonic Waveguides, *Phys. Rev. Lett.*, 2004, **93**, 137404.
6 V. Giannini, A. I. Fernández-Domínguez, S. C. Heck and S. A. Maier, Plasmonic Nanoantennas: Fundamentals and Their Use in Controlling the Radiative Properties of Nanoemitters, *Chem. Rev.*, 2011, **111**, 3888–3912.
7 *Metal clusters*, Wiley series in theoretical chemistry, ed. W. Ekardt, John Wiley & Sons Ltd, Chichester, 1999.
8 G. F. Bertsch, A. Bulgac, D. Tomanek and Y. Wang, Collective plasmon exitation in C_{60} Clusters, *Phys. Rev. Lett.*, 1991, **67**, 2690.
9 I. V. Hertel, H. Steger, J. de Vries, B. Weisser, C. Menzel and B. Kamke, *et al.*, Giant plasmon excitation in free C_{60} and C_{70} molecules studied by photoionization, *Phys. Rev. Lett.*, 1992, **68**, 784–787.
10 K. Selby, M. Vollmer, J. Masui, V. Kresin, W. de Heer and W. D. Knight, Surface plasma resonances in free metal clusters, *Phys. Rev. B: Condens. Matter Mater. Phys.*, 1989, **40**, 5417.
11 S. Pollack, C. R. C. Wang and M. M. Kappes, On the optical response of Na_{20} and its relation to computational prediction, *J. Chem. Phys.*, 1991, **94**, 2496–2501.
12 C. Bréchignac, P. Cahuzac, N. Kebaili, J. Leygnier and A. Sarfati, Collective Resonances in Large Potassium Cluster Ions, *Phys. Rev. Lett.*, 1992, **68**, 3916–3919.
13 C. Bréchignac, P. Cahuzac, J. Leygnier and A. Sarfati, Optical Response of large Lithium Clusters: Evolution towards the bulk, *Phys. Rev. Lett.*, 1993, **70**, 2036–2039.
14 T. Reiners, C. Ellert, M. Schmidt and H. Haberland, Size Dependence of the Optical Response of Spherical Sodium Clusters, *Phys. Rev. Lett.*, 1995, **74**, 1558–1561.
15 W. Ekardt, Work function of small metal particles: Self consistent spherical jellium-background model, *Phys. Rev. B: Condens. Matter Mater. Phys.*, 1984, **29**, 1558–1564.
16 W. A. de Heer, The Physics of Simple Metal Clusters: Experimental Aspects and Simple Models, *Rev. Mod. Phys.*, 1993, **65**, 611.
17 F. Abeles, *Optical Properties of Solids*, North-Holland Publishing, London, 1972.
18 K. Selby, V. Kresin, J. Masui, M. Vollmer, W. A. de Heer and A. Scheidemann, *et al.*, Photoabsorption spectra of sodium clusters, *Phys. Rev. B: Condens. Matter Mater. Phys.*, 1991, **43**, 4565.
19 C. Bréchignac, P. Cahuzac, F. Carlier, M. deFrutos and J. Leygnier, Optical Excitation in small ionized sodium Clusters: Closed-Shell and Open-Shell systems, *Chem. Phys. Lett.*, 1992, **189**, 28–34.
20 C. Ellert, M. Schmidt, C. Schmitt, T. Reiners and H. Haberland, Temperature Dependence of the Optical Response of Small, Open Shell Sodium Clusters, *Phys. Rev. Lett.*, 1995, **75**, 1731–1734.
21 H. Fallgren, K. M. Brown and T. P. Martin, Photoabsorption spectra of Cs_N O and Cs_N clusters, *Z. Phys. D: At., Mol. Clusters*, 1991, **19**, 81.
22 W. Ekardt, Size-dependent photoabsorption and photoemission of small metal particles, *Phys. Rev. B: Condens. Matter Mater. Phys.*, 1985, **31**, 6360.
23 V. Bonacic-Koutecký, P. Fantucci and J. Koutecký, Theoretical interpretation of the photoelectron detachment spectra of Na_{2-5} and of the absorption spectra of Na_3, Na_4, and Na_8 clusters, *J. Chem. Phys.*, 1990, **93**, 3802–3825.
24 P. G. Reinhard, O. Genzken and M. Brack, From sum rules to RPA: 3. Optical dipole response in metal clusters, *Ann. Phys.*, 1996, **5**, 576–607.
25 J. M. Pacheco and J. L. Martins, Ab initio pseudopotential calculation of the photo-response of metal clusters, *J. Chem. Phys.*, 1997, **106**, 6039–6044.
26 K. P. Charlé, L. König, S. Nepijko, I. Rabin and W. Schulze, The Surface Plasmon Resonance of Free and Embedded Ag-Clusters in the Size Range 1,5 nm $<$ D $<$ 30 nm, *Cryst. Res. Technol.*, 1998, **33**, 1085–1096.
27 J. Tiggesbäumker, L. Köller, K. H. Meiwes-Broer and A. Liebsch, Blue Shift of the Mie Plasma Frequency in Ag Clusters and Particles, *Phys. Rev. A: At., Mol., Opt. Phys.*, 1993, **48**, R1749–R1752.
28 K. Baishya, J. C. Idrobo, S. Öğüt, M. Yang, K. A. Jackson and J. Jellinek, First-principles absorption spectra of Cu_n (n = 2 − 20) clusters, *Phys. Rev. B: Condens. Matter Mater. Phys.*, 2011, **83**, 245402.
29 B. Anak, M. Bencharif and F. Rabilloud, Time-dependent density functional study of UV-visible absorption spectra of small noble metal clusters (Cu_n, Ag_n, Au_n, n = 2-9, 20), *RSC Adv.*, 2014, **4**, 13001–13011.
30 J. Tiggesbäumker, L. Köller and K. H. Meiwes-Broer, Bound-free collective electron excitations in negatively charged silver clusters, *Chem. Phys. Lett.*, 1996, **260**, 428–432.
31 T. Reiners and H. Haberland, Plasmon Enhanced Electron and Atom Emission from a Spherical Sodium Cluster: Na_{91}^-, *Phys. Rev. Lett.*, 1996, **77**, 2440–2443.
32 K. Raspe, M. Müller, N. Iwe, R. N. Wolf, P. OelÃŸner and F. Martinez, *et al.*, A versatile setup for studying size and charge-state selected polyanionic nanoparticles, *Rev. Sci. Instrum.*, 2022, **93**, 043301.
33 H. Haberland, *1. In: History, Some Basics, and an Outlook*, John Wiley & Sons, Ltd, 2017, p. 1–21.
34 F. Martinez, S. Bandelow, C. Breitenfeldt, G. Marx, L. Schweikhard and A. Vass, *et al.*, Upgrades at ClusterTrap and latest results, *Int. J. Mass Spectrom.*, 2014, **365–366**, 266–274.

35 P. Kruit and F. H. Read, Magnetic field paralleliser for 2π electron-spectrometer and electron-image magnifier, *J. Phys. E: Sci. Instrum.*, 1983, **16**, 313.
36 N. Iwe, K. Raspe, M. Müller, F. Martinez, L. Schweikhard and K. H. Meiwes-Broer, *et al.*, Size and charge-state dependence of detachment energies of polyanionic silver clusters, *J. Chem. Phys.*, 2021, **155**, 164303.
37 O. Kostko, Photoelectron spectroscopy of mass-selected sodium, coinage metal and divalent metal cluster anions. *University of Freiburg*, 2007.
38 J. Tiggesbäumker, L. Köller, H. O. Lutz and K. H. Meiwes-Broer, Giant resonances in silver-cluster photofragmentation, *Chem. Phys. Lett.*, 1992, **190**, 42–47.
39 F. Federmann, K. Hoffmann, N. Quaas and J. P. Toennies, Spectroscopy of extremly cold silver clusters in helium droplets, *Eur. Phys. J. D*, 1999, **9**, 11–14.
40 T. Diederich, J. Tiggesbäumker and K. H. Meiwes-Broer, Spectroscopy on rare gas-doped silver clusters in helium droplets, *J. Chem. Phys.*, 2002, **116**, 3263–3269.
41 H. Hövel, S. Fritz, A. Hilger, U. Kreibig and M. Vollmer, Width of cluster plasmon resonances: Bulk dielectric functions and chemical interface damping, *Phys. Rev. B: Condens. Matter Mater. Phys.*, 1993, **48**, 18178–18188.
42 E. Loginov, L. F. Gomez, N. Chiang, A. Halder, N. Guggemos and V. V. Kresin, *et al.*, Photoabsorption of Ag_N(N$\sim$ 6 − 6000) Nanoclusters Formed in Helium Droplets: Transition from Compact to Multicenter Aggregation, *Phys. Rev. Lett.*, 2011, **106**, 233401.
43 S. Saito, G. F. Bertsch and D. Tománek, Collective electronic excitations in small metal clusters, *Phys. Rev. B: Condens. Matter Mater. Phys.*, 1991, **43**, 6804–6807.
44 F. Federmann, K. Hoffmann, N. Quaas and J. D. Close, Rydberg states of silver: Excitation dynamics of doped helium droplets, *Phys. Rev. Lett.*, 1999, **83**, 2548–2551.
45 J. Lehmann, M. Merschdorf, W. Pfeiffer, A. Thon, S. Voll and G. Gerber, Surface Plasmon Dynamics in Silver Nanoparticles Studied by Femtosecond Time-Resolved Photoemission, *Phys. Rev. Lett.*, 2000, **85**, 2921–2924.
46 U. Hild, G. Dietrich, S. Krückeberg, M. Lindinger, K. Lützenkirchen and L. Schweikhard, *et al.*, Time-resolved photofragmentation of stored silver clusters Ag_n^+, *Phys. Rev. A: At., Mol., Opt. Phys.*, 1998, **57**, 2786–2793.
47 K. Hansen, A. Herlert, L. Schweikhard and M. Vogel, Dissociation energies of silver clusters Ag_n^+, n = 14, 15, 16, 18, *Int. J. Mass Spectrom.*, 2003, **227**(1), 87–96.
48 L. Schweikhard, G. Dietrich, U. Hild, S. Krückeberg, K. Lützenkirchen and C. Walther, Pulsed photodissociation in an ion cyclotron resonance trap: extending the time range for unimolecular dissociation studies of metal clusters, *Rapid Commun. Mass Spectrom.*, 1997, **11**, 1624–1626.
49 Y. Shi, V. A. Spasov and K. M. Ervin, Competitive fragmentation and electron loss kinetics of photoactivated silver cluster anions: Dissociation energies of Ag_n^- (n = 7-11), *J. Chem. Phys.*, 1999, **111**, 938–949.
50 R. Kubo, Electronic Properties of Metallic Fine Particles. I, *J. Phys. Soc. Jpn.*, 1962, **17**, 975–986.
51 G. Mourou, Nobel Lecture: Extreme light physics and application, *Rev. Mod. Phys.*, 2019, **91**, 030501.
52 D. M. Neumark, Time-resolved photoelectron spectroscopy of molecules and clusters, *Annu. Rev. Phys. Chem.*, 2001, **52**, 255–278.
53 J. R. R. Verlet, Femtosecond spectroscopy of cluster anions: insights into condensed-phase phenomena from the gas-phase, *Chem. Soc. Rev.*, 2008, **37**, 505–517.
54 B. A. Collings, K. Athanassenas, D. M. Rayner and P. A. Hackett, Optical spectroscopy of Ag_7, Ag_9^+, and Ag_9. A test of the photodepletion method, *Chem. Phys. Lett.*, 1994, **227**, 490–495.
55 A. Terasaki, T. Majima, C. Kasai and T. Kondow, Photon-trap spectroscopy of size-selected free cluster ions: direct measurement of optical absorption of Ag_9^+, *Eur. Phys. J. D*, 2009, **52**, 43–46.
56 T. Lünskens, P. Heister, M. Thämer, C. A. Walenta, A. Kartouzian and U. Heiz, Plasmons in supported size-selected silver nanoclusters, *Phys. Chem. Chem. Phys.*, 2015, **17**, 17541–17544.
57 C. Yu, R. Schira, H. Brune, B. von Issendorff, F. Rabilloud and W. Harbich, Optical properties of size selected neutral Ag clusters: electronic shell structures and the surface plasmon resonance, *Nanoscale*, 2018, **10**, 20821–20827.
58 L. Serra and A. Rubio, Optical response of Ag clusters, *Z. Phys. D: At., Mol. Clusters*, 1997, **40**, 262–264.
59 V. Kasperovich and V. V. Kresin, Ultraviolet photoabsorption spectra of silver and gold nanoclusters, *Philos. Mag. B*, 1998, **78**, 385–396.
60 V. Bonačić-Koutecký, V. Veyret and R. Mitric, Ab initio study of the absorption spectra of AgN (N = 5 − 8) clusters, *J. Chem. Phys.*, 2001, **115**, 10450–10460.
61 E. Cottancin, G. Celep, J. Lermé, M. Pellarin, J. R. Huntzinger and J. L. Vialle, *et al.*, Optical Properties of Noble Metal Clusters as a Function of the Size: Comparison between Experiments and a Semi-Quantal Theory, *Theor. Chem. Acc.*, 2006, **116**, 514–523.
62 K. Baishya, J. C. Idrobo, S. Öğüt, M. Yang, K. Jackson and J. Jellinek, Optical absorption spectra of intermediate-size silver clusters from first principles, *Phys. Rev. B: Condens. Matter Mater. Phys.*, 2008, **78**, 075439.
63 F. Rabilloud, UV-visible absorption spectra of metallic clusters from TDDFT calculations, *Eur. Phys. J. D*, 2013, **67**, 18.
64 M. Kuisma, A. Sakko, T. P. Rossi, A. H. Larsen, J. Enkovaara and L. Lehtovaara, *et al.*, Localized surface plasmon resonance in silver nanoparticles: Atomistic first-principles time-dependent density-functional theory calculations, *Phys. Rev. B: Condens. Matter Mater. Phys.*, 2015, **91**, 115431.
65 J. T. Titantah and M. Karttunen, Ab initio calculations of optical properties of silver clusters: cross-over from molecular to nanoscale behavior, *Eur. Phys. J. B*, 2016, **89**, 125.
66 G. U. Kuda-Singappulige and C. M. Aikens, Excited-State Absorption in Silver Nanoclusters, *J. Phys. Chem. C*, 2021, **125**, 24996–25006.
67 M. Mucke, M. Förstel, T. Lischke, T. Arion, A. M. Bradshaw and U. Hergenhahn, Performance of a short magnetic bottle electron spectrometer, *Rev. Sci. Instrum.*, 2012, **83**, 063106.

68 J. Li, X. Li, H. J. Zhai and L. S. Wang, Au_{20}: A Tetrahedral Cluster, *Science*, 2003, **299**, 864–867.
69 L. Brus, Noble Metal Nanocrystals: Plasmon Electron Transfer Photochemistry and Single-Molecule Raman Spectroscopy, *Acc. Chem. Res.*, 2008, **41**, 1742–1749.
70 W. Hou and S. B. Cronin, A Review of Surface Plasmon Resonance-Enhanced Photocatalysis, *Adv. Funct. Mater.*, 2013, **23**, 1612–1619.
71 S. Pillai and M. A. Green, Plasmonics for photovoltaic applications, *Sol. Energy Mater. Sol. Cells*, 2010, **94**, 1481–1486.

